On the resolution of density anomalies in the Earth's mantle using spectral fitting of normal mode data

Chaincy Kuo[1] and Barbara Romanowicz
Department of Geology and Geophysics, University of California, Berkeley, California, USA

submitted to Geophysical Journal International
in original form 2000 August 1

Abbreviated title: "On the resolution of mantle density..."

Corresponding author: Chaincy Kuo, Lawrence Berkeley National Laboratory, 1 Cyclotron Road, MS 55-121, Berkeley, CA, 94720, USA; Phone: +1-510-486-6762; FAX: +1-510-486-4768; Email: CKuo@lbl.gov.

[1] Now at E. O. Lawrence Berkeley National Laboratory, Berkeley, California, USA

Abstract. The resolution of the three-dimensional density structure in the Earth's deep interior has long eluded geoscientists. High quality data from digital seismic instruments emplaced this decade have renewed interest in the measurement of low frequency Earth normal modes with the goal of extracting the heterogeneous density structure (*Ishii and Tromp, 1999; Kuo and Romanowicz, 1999a,b; Resovsky and Ritzwoller, 1999*). We here perform a series of synthetic experiments aimed at investigating the resolution of lateral variations in the mantle from normal mode spectral data. Contamination effects between seismic velocities and density are examined in two ways: 1) by using resolution matrices computed from data kernels, and 2) by inverting synthetic spectra computed from realistic input Earth models. These resolution tests indicate that density structure retrieved from presently available normal mode data is not reliable. Contamination of seismic velocity structure into the density model space produces patterns which resemble those obtained from inversions of real data. The resulting density models appear to be dependent on a combination of the starting velocity models and the model parameterization.

Key words: Mantle, density, normal modes, seismic tomography

Introduction

The issue of whether lateral variations in density in the mantle can be resolved from normal mode data has recently received renewed attention, in particular with the work of *Ishii and Tromp* (1998, 1999). In their recently published paper, these authors present a degree 6 model of density throughout the mantle, derived from inversion of normal mode splitting coefficients. This model presents unexpected features in the lowermost mantle, namely two large "blobs" of high density material centered in the Pacific and under Africa, that, if real, could have important consequences for the dynamics of the mantle. *Ishii and Tromp* (1999) argue for the robustness of their model, on the basis of numerous experiments, including checkerboard resolution tests and exploration of different parameterization schemes.

Whether lateral variations in density can be resolved from normal mode data has long been the subject of debate. *Resovsky and Ritzwoller* (1999) have recently presented the results of tests which show that the retrieved density structure is very sensitive to the regularization scheme used in the inversion. Imposed *a priori* constraints on the location and size of density heterogeneity have a strong effect on the resulting models, which, while providing equal fit to the data, can be significantly different. *Ishii and Tromp* (1999) however, argue that their density model is weakly dependent on their starting model.

In what follows, we present the results of a series of tests in which we have explored more fully the structure of the resolution matrix than can be obtained with checkerboard tests. Because, in the case of non-linear inversions, the resolution matrix approach only allows us to investigate the problem approximately, we also present results of tests in which we compute synthetic seismograms for realistic Earth models and invert them under the same conditions as the real data.

In the experiments presented here we use a synthetic data set and inversion scheme that mimics the actual data set and methodology which we have used in a study of 3D mantle structure based on real mode data (*Kuo and Romanowicz, 1999; Kuo, 1999*).

This mode data set comprises the spectra of 44 speroidal modes observed on the vertical component, including 7 pairs of coupled modes that provide some sensitivity to odd degree structure. The analysis method is a one-step inversion scheme in which mantle structure in V_s, V_p and ρ is derived directly from the observed spectra. This contrasts with the approach of some recent studies, which use a two step procedure, involving the computation of splitting coefficients followed by an inversion for 3D structure (*eg. Ishii and Tromp, 1999; Resovsky and Ritzwoller, 1999*).

Tests with resolution matrices

Resolution matrix

The resolution matrix is a useful tool to assess the leakage between model parameters in a generalized inversion framework. Indeed, the solution $\mathbf{m}_{est}$ to the inverse problem $\mathbf{d_{obs}} = \mathbf{A}\mathbf{m}$, where $\mathbf{A}$ is a linearized data kernel, $\mathbf{d_{obs}}$ is the data vector, and $\mathbf{m}$ the model vector, can be written as:

$$\mathbf{m}_{est} = (\mathbf{A}^T\mathbf{A} + \mathbf{C}_m^{-1})^{-1}\mathbf{A}^T\mathbf{d}_{obs} \tag{1}$$

where $\mathbf{C}_m^{-1}$ is the matrix of damping parameters. The relation between the vector of estimated model parameters $\mathbf{m}_{est}$ and the true model $\mathbf{m}_{true}$, for a given parameterization and underlying theory, is then:

$$\mathbf{m}_{est} = (\mathbf{A}^T\mathbf{A} + \mathbf{C}_m^{-1})^{-1}\mathbf{A}^T\mathbf{A}\mathbf{m}_{true}. \tag{2}$$

The $M \times M$ model resolution matrix $\mathbf{R}$, where M is the number of unknown parameters, is defined as

$$\mathbf{R} = (\mathbf{A}^T\mathbf{A} + \mathbf{C}_m^{-1})^{-1}\mathbf{A}^T\mathbf{A} \tag{3}$$

so that

$$\mathbf{m}_{est} = \mathbf{R}\mathbf{m}_{true}. \tag{4}$$

If $\mathbf{R} = \mathbf{I}$, where $\mathbf{I}$ is the identity matrix, then each model parameter is perfectly resolved.

In practice, $\mathbf{R} = \mathbf{I}$ has non zero off-diagonal terms, and their size relative to each other and to the diagonal terms indicates the amount of contamination (or "covariance") between the different parameters as determined by inversion.

In our particular problem, we invert simultaneously for structure in V_P, V_S and ρ, and wish to investigate the level of contamination between these parameters. The model vector is arranged as follows:

$$\mathbf{m} = [\,{}_pV^t_{P\,s},\ {}_pV^t_{S\,s},\ {}_p\rho^t_s], \tag{5}$$

where the indices s, t, p refer to the parameterization of the model. In our studies, we have chosen spherical harmonics as basis functions in the horizontal direction, and Legendre polynomials in the vertical direction. The maximum degree ($s_{max} = 6$) of the spherical harmonics expansion is chosen in view of the sensitivity of the particular mode data set we are considering, given that a particular mode of angular order l is sensitive to at most lateral heterogeneity of degree $2l$. The maximum order of the radial polynomial expansion is commensurate with the maximum radial order n of the modes in our data set ($p_{max} = 7$). We will compare results for $p_{max} = 7$ and $p_{max} = 10$, as it has been argued (e.g. *Ishii and Tromp, 1999*) that more stable results can be obtained by overparameterizing the model and then damping more strongly.

The resolution equation is then:

$$\begin{bmatrix} {}_pV^t_{P\,s} \\ {}_pV^t_{S\,s} \\ {}_p\rho^t_s \end{bmatrix}_{est} = \begin{bmatrix} R_P & \emptyset_{SP} & \emptyset_{RP} \\ \emptyset_{PS} & R_S & \emptyset_{RS} \\ \emptyset_{PR} & \emptyset_{SR} & R_R \end{bmatrix} \begin{bmatrix} {}_pV^t_{P\,s} \\ {}_pV^t_{S\,s} \\ {}_p\rho^t_s \end{bmatrix}_{true} \tag{6}$$

where R_P, R_S, and R_R are resolution submatrices for ${}_pV^t_{P\,s}$, ${}_pV^t_{S\,s}$, and ${}_p\rho^t_s$ respectively, and non-zero values in $\emptyset_{PS}$ are the covariances which would map V_P structure into V_S structure, and so on. The $\emptyset$'s are zero in an ideal resolution matrix.

Imposing *a priori* distributions. Since the resolution matrix is a function of both the data kernels and the *a priori* model covariance matrix, C_m^{-1}, it is important to carefully choose the *a priori* damping parameters so as to obtain, inasmuch as possible,

$\mathbf{R} \approx \mathbf{I}$.

To do so, we consider a "realistic" synthetic model, for which we choose S velocity (V_S) to be that of model SAW12D (*Li and Romanowicz, 1996*), and P velocity (V_P)to be that of P16B30 (*Masters et al, 1996*). A mock density model (ρ) is constructed so that the root-mean-square amplitudes are about 25% of V_S, a common assumption in low-frequency seismology (e.g. *Li et al., 1991*) that is in agreement with laboratory measurements at shallow mantle pressure and temperatures (*Karato, 1993*). The mock density perturbations are constructed by permuting and scaling (to 25%) coefficients of V_s model SAW12D so that the actual patterns of heterogeneity are not correlated with SAW12D, and we name this model R25. As mentioned previously, we consider two different spatial parameterizations: 1) $s_{max} = 6, p_{max} = 7$ (Experiment A), and 2) $s_{max} = 6, p_{max} = 10$ (Experiment B). The resolution matrix is computed using the data kernels corresponding to our data set of 44 spheroidal mode spectra.

Damping parameters are defined separately for $\delta V_P, \delta V_S$, and $\delta\rho$ and chosen in such a fashion as to best recover the rms amplitudes of the true model for even degrees (2,4,6) after applying the resolution matrix. We only consider norm damping (η_1) and we find that values of $\eta_1^P = \eta_1^S = \eta_1^R = 1$ are adequate for both spatial parameterizations (Figs 1a and c). The odd degree structure amplitudes are slightly overestimated due to the inadequate constraints from only two mode pairs (${}_1S_4 - {}_2S_5$ and ${}_1S_5 - {}_2S_6$) for degrees 1, 3, and 5, and three mode pairs (${}_4S_3 - {}_2S_8$, ${}_6S_3 - {}_3S_8$, and ${}_2S_{10}\,{}_4S_5$) for degree 5 only. It is interesting to note that in the depth ranges in which the rms amplitudes in δV_P and δV_S are decreased, the amplitudes in $\delta\rho$ are increased (400-1200 km, and 1600-2400 km depth), potentially indicating leakage from the former to the latter. In Figs 1b and d, the correlations between $\mathbf{m}_{true}$ and $\mathbf{m}_{est}$ are plotted for spatial parameterizations $s_{max} = 6, p_{max} = 7$, and $s_{max} = 6, p_{max} = 10$ respectively. We recover perturbations in V_P and V_S well for the spatial parameterization $s_{max} = 6, p_{max} = 7$, (correlation coefficients of 75%-99%), and perturbations in ρ are recovered with ~60% correlation. For the spatial parameterization $s_{max} = 6, p_{max} = 10$, we can still recover perturbations in V_P and V_S sufficiently, although in the depth range 400-670 km, the correlation drops to ~50%. Perturbations in ρ at the top of the lower mantle are poorly recovered in this parameterization. Clearly, adding vertical smoothing is necessary to compensate for overparameterization in the vertical direction.

If the patterns of perturbation in our input model $\mathbf{m}_{true}$ are the same for δV_s, δV_p, and ρ , then a resolution experiment on such an $\mathbf{m}_{true}$ is insufficient to assess the leakage of V_S and V_P structure into ρ. However, it gives us an opportunity to examine the structure of the resolution matrix, which is independent of the input model coefficients. The resolution matrix is presented in Figure 2, which shows that the part of the matrix corresponding to V_S and V_P has a structure close to that of an identity matrix, with strongest values on the diagonal, and generally weak cross-terms $\emptyset_{SP}$ and $\emptyset_{PS}$. On the other hand, the density sub-matrix shows both much smaller values on the diagonal, compared to V_S and V_P, and off-diagonal terms $\emptyset_{RP}$, $\emptyset_{RS}$... which are small but commensurate with the diagonal terms. The structure of the resolution matrix indicates that density cannot be resolved as well as velocity structure. The relative level of damping between velocities and density will only act to scale the off-diagonal terms with the diagonal terms, and therefore contamination will always be present.

Many authors perform checkerboard tests to assess the resolution of their models. In this kind of test, the model vector $\mathbf{m}_{true}$ is sparsely populated by non zero coefficients ${}_pm_s^t$. For example, a checkerboard model of $s = 4$, $t = 4$, and $p = 7$ will consist of non-zero values for ${}_pm_4^4$ and ${}_pm_4^{-4}$ for $0 \leq p \leq 7$. This gives 16 non-zero elements in $\mathbf{m}_{true}$, of dimension $M = 200$ ($M = (s+1)^2(p+1)$). The remaining 184 elements of $\mathbf{m}_{true}$ are zero. Then, many non-zero off-diagonal elements in $\mathbf{R}$ can be neutralized by the product with zero or very small valued elements in $\mathbf{m}_{true}$, and the covariances in $\mathbf{R}$ may not be found by this type of test, even if it is performed at several degrees s.

Also, one may introduce a checkerboard model for δV_P only, where $\delta V_S = 0$ and $\delta\rho = 0$ in $\mathbf{m}_{true}$, to analyze the possible mapping of V_P structure into V_S and ρ structure, or introduce a checkerboard pattern for δV_S only to analyze the possible mapping of V_S structure into V_P and ρ structure, and so on (*Ishii and Tromp, 1999*). Then, for a checkerboard pattern $s = 4$, $t = 4$, and $p = 7$ in only one physical parameter vector, there are 16 non-zero values populating $\mathbf{m}_{true}$ of dimension $M = 600$ ($M = (s+1)^2(p+1) \times 3$). Off-diagonal elements in $\mathbf{R}$ can be missed, unless checkerboard tests are run for each model coefficient, which is not generally done. Even so, if all coefficients are explored, small amounts of contamination into other model parameters may be observed for each coefficient and may be deemed neglible. In this case, the cumulative contamination of all coefficients from one model parameter into a particular coefficient of another model parameter is not assessed, nor is the pattern of the cumulative contamination. In other words, the mapping between physical parameters is not fully explored.

Instead of using a checkerboard model, in a first set of experiments, we choose to fully populate δV_P (respectively δV_S and $\delta\rho$) with coefficients of an aspherical model, keeping the other parameters zero. We can thus test how well we can resolve each parameter, independently of the others, and how much is mapped into the others. Our input models are therefore, respectively $\mathbf{m}^P_{true} = [\delta V_P, \emptyset, \emptyset]$ $\mathbf{m}^S_{true} = [\emptyset, \delta V_S, \emptyset]$ and $\mathbf{m}^R_{true} = [\emptyset, \emptyset, \delta\rho]$. The same model of heterogeneity is used in all three cases, but the amplitudes are scaled according to V_P =0.5 V_S, and $\rho = 0.25$ V_S, to achieve realistic rms levels in the respective parameters being tested. Resolution experiments with parameterizations A and B, as defined above, are performed in each case.

In Figures 3– 5, we plot the results of the three resolution tests using $\mathbf{m}^P_{true}$, $\mathbf{m}^S_{true}$, and $\mathbf{m}^R_{true}$ respectively for $s_{max} = 6, p_{max} = 7$. The legend scale for heterogeneity for $\delta \ln V_P$ is ±1%, for δV_S is ±1.5%, and for $\delta\rho$ is ±0.5%. The color scale is chosen so as to correspond to expected amplitudes for each physical parameter. Figure 3 shows that δV_P is well recovered, but there is some contamination into $\delta V_{S\,est}$ and $\delta\rho_{est}$, as expected from the visualization of $\mathbf{R}$. The amplitude of contamination into $\delta V_{S\,est}$ is very small, and is well below the level of signal obtained in real data inversions, so it should not be a problem. The amplitude of contamination into $\delta\rho_{est}$ is also not very large, but patterns at certain depths, particularly at 2800 km, are reminiscent of patterns from recent density models inverted from normal mode splitting coefficients (*Ishii and Tromp, 1999*), where high density features are located over Africa, and the Pacific basin region. In the upper mantle, there is significant contamination of δV_P

patterns into $\delta\rho$. In Figure 4, δV_S is well resolved, with insignificant contamination into ${\delta V_P}_{est}$. The contamination amplitude into $\delta\rho_{est}$ is somewhat higher, and the patterns mapped into the density model appear as high densities in areas of slab subduction in the circum-Pacific regions, especially at the bottom of the mantle. In the upper mantle, the same patterns of contamination in $\delta\rho$ from δV_S appear as in Figure 3, but at somewhat stronger amplitudes. Finally, in Figure 5, we see that $\delta\rho$ can be recovered in the absence of δV_S and δV_P structure, and there is not significant contamination into ${\delta V_P}_{est}$ and ${\delta V_S}_{est}$ in amplitude and pattern.

The results of an analogous experiment are shown in Figures 6-8 for spatial parameterization $s_{max} = 6, p_{max} = 10$, and the contamination effects are similar to the effects for spatial parameterization $s_{max} = 6, p_{max} = 7$.

Cumulative contamination

As seismic velocity structure in the Earth is relatively well-documented (*Su et al., 1994; Li and Romanowicz, 1996; Masters et al, 1996; Dziewonski et al, 1997; Vasco and Johnson, 1997; van der Hilst et al., 1997*), the study of cumulative contamination of δV_P and δV_S into $\delta\rho$ can be particularly informative. To investigate the latter, we have performed a series of tests (labeled C-J), in which we vary the depth parameterization ($p_{max} = 7$ versus $p_{max} = 10$) and the input δV_S model, keeping the input model in ρ to be zero. Table 1 describes the details of each experiment.

The comparison of the models obtained in experiments C,D (same initial models, different depth parameterization) with those of experiments A and B respectively, indicates that the velocity structures are well recovered, but a spurious density structure is introduced in C,D. This density structure is well correlated with that obtained in A, B, where the starting model was a realistic density model (Figs 9b and d). The maps of 'ghost' density patterns for degrees 2, 4, and 6 are shown in Figs 10a and b for Experiments C and D. Only the even degrees are displayed to compare directly with published density models, even though the odd degree model parameters are not very large and do not have much of an impact on the displayed images. High density regions corresponding to regions of slab subduction exist at many depths. In fact, the patterns of $\delta\rho^{C}_{est}$ and $\delta\rho^{C}_{est}$ are similar to density models obtained from inversions of spectral data, which we call R_NMSPEC (Fig. 10c)(*Kuo et al., 1998; Kuo and Romanowicz, 1999a,1999b*). The model R_NMSPEC is spatially parameterized to $s_{max} = 6$ and $p_{max} = 7$, and no *a priori* assumptions are imposed for the inversion of observed spectral data. The correspondence between Figs 10a and c shows that if P16B30 and SAW12D are representative of the seismic velocity perturbations in the real Earth, the artifact density models puts into question the confidence we have in the density models obtained from the inversions of the normal mode spectra. Although the amplitudes of the artifact density models are much smaller than the density features in models derived from real data, the similarity in pattern cannot be ignored, given that mantle density structure is not well-established. We will show in a following section that artifact density amplitudes derived from inversions of synthetic data are commensurate with amplitudes obtained using the real data.

If we use SH12WM13 (*Su and Dziewonski, 1994*), as a starting model for δV_S, (experiments E-F), the ghost density model retrieved is somewhat different. In Experiment F, the resulting ghost density model for a $s_{max} = 6, p_{max} = 10$ parameterization yields patterns which are strongly reminiscent of the published density model SPRD6 of *Ishii and Tromp* (1999) , particularly the high density feature in the Pacific basin and over Africa at 2800 km. From Figs 11b and c, the density patterns from $\delta\rho^{F}_{est}$ and SPRD6 (*Ishii and Tromp, 1999*) can be directly compared for six depths in the mantle. The resemblance is striking, although the amplitudes of $\delta\rho^{F}_{est}$ are much smaller in the lower mantle, and there are slight lateral shifts in the distribution of the patterns between $\delta\rho^{F}_{est}$ and $\delta\rho_{est}$ of SPRD6 (*Ishii and Tromp, 1999*) . However, amplitudes retrieved from inversions are dependent on the choice of damping parameter values. There is not so much resemblance to the SPRD6 density model for the $p_{max} = 7$ parameterization in Experiment E (Fig. 11a), but high density ghost features also appear in the Pacific Basin at 2800 km. The source of this contamination could be attributed to δV_P (Figures 3 and 6, if one assumes that V_p is highly correlated with V_s).

While regularization schemes used in resolution tests are not directly applicable to the inversion of observed data (*Resovsky and Ritzwoller, 1999*) due to the effects of noise, the damping scheme which we use is quite simplistic in $\mathbf{C}_m^{-1}$ and is imposed in the absence of noise. Despite this simplistic damping scheme, we can retrieve ghost density models which mimic density models inverted from data. Tests of model robustness by considering random noise in the data (*Ishii and Tromp, 1999*) can still stably produce density models such as in Fig. 11b since the contamination in the density model parameter space is due to coherent rather than random noise. Tests involving random noise to quantitatively understand its effects against this kind of coherent noise will be performed in the future.

Of course, the contamination effect is more important for a low level of signal in $\delta\rho_{true}$, and for larger levels of signal in ρ, it may still be possible to retrieve some information, especially by applying an appropriate damping scheme. However, the confidence in the resulting model will always be marginal since we do not *a priori* know the level of density heterogeneity in the real Earth, in the absence of sufficient mineral physics information. Confidence tests may require supplementation by independent information, such as constraints provided by fits to the observed geoid.

Tests with ρ input models of different amplitudes

Experiments A-F have demonstrated that density perturbation amplitudes which are about 25% of δV_s cannot be retrieved with confidence. The estimated models of density in Experiments A and B, in which a mock input density model is used, are highly correlated with the estimated densities of Experiments C and D, for which no input density was used. The high correlation demonstrates that contamination from seismic velocity signal swamps out the density signal in Experiments A and B. The level of density perturbation signal in the Earth which can be detected needs to be investigated. To do so we refer to experiments A,B and H,I (Table 1) in which we respectively consider two input density models which differ only by an amplitude scaling factor. The mock density perturbations in model R50 have twice the amplitudes as in model R25.

At the level of density signal in R50, Fig. 12b shows that input $\delta\rho^H_{true}$ is correlated with output $\delta\rho^H_{est}$ much better than when the density signal is that of R25 (Fig. 1b), indicating that density can be resolved better for R50 than for R25. Overall, this is true for the correlation of $\delta\rho^I_{true}$ and $\delta\rho^I_{est}$ in comparison with the correlation of $\delta\rho^B_{true}$ and $\delta\rho^B_{est}$ (Figs 12d and 1d), but for this radial parameterization, $p_{max} = 10$, the density correlation in Experiment I is poor below the transition zones down to 1200 km depth. This indicates that Experiment I is overparameterized, leading to deficiencies in resolution.

Next, we correlate the $\delta\rho_{est}$'s in Experiments H and I with ghost density estimates from Experiments C and D. Correlation of $\delta\rho^H_{est}$ with the ghost density model $\delta\rho^C_{est}$ is decreased in comparison with Fig. 9b, as shown in Fig. 13a. However, $\delta\rho^I_{est}$ correlates above 50% with the ghost density model $\delta\rho^D_{est}$ in over three-fourths of the mantle, shown in Fig. 13b.

These tests demonstrate that for the 44 spheroidal modes which we use in our data set, the radial parameterization $p_{max} = 7$ can begin to retrieve density patterns over the contamination signal if the amplitudes of density perturbations are 50% of the V_s perturbation amplitudes, that is, a little less than 2% for $\delta\rho/\rho$ in the shallow mantle. In addition, models parameterized to higher orders, such as $p_{max} = 10$, suffer in resolving power if not sufficiently damped. It is not inconceivable that actual density fluctuations would differ by as much as a factor of two compared to the results of laboratory measurements (eg., *Karato, 1993*).

Although the density models obtained from normal mode data (*Ishii and Tromp, 1999; Kuo and Romanowicz, 1999*) currently resemble the ghost density patterns from Experiments C-F, the Earth's 3D density structure could still be resolved, if the perturbations are large enough. The expected amplitude of density perturbations due to slabs at high pressures and temperatures (*Panero and Jeanloz, in preparation*) is 1-2%. If the localized inclusions suggested by the high pressure and temperature experiments are pervasive in the mantle, then they may constitute large scale structure to which the modes may be sensitive. Then, the density signal may be at the limit of being resolvable. If there is real signal in the density models derived from data, it may very likely be overwhelmed by contamination. The plots in Figs 9a and 9c show that the contaminant density amplitudes can be commensurate with the amplitudes in R50 (left plot in Fig. 12a). Inversions with real data can yield density amplitudes greater than those in R50, but before assuming that the amplitudes are an indication of large signal, one must ensure that the amplitudes are not due to coherent errors from contamination producing such an amplified signal. It will be necessary to find appropriate damping parameters to reduce the effect of the covariant elements between physical model parameters in the resolution matrix.

Tests with synthetic seismograms

So far, we have only considered simple tests, to illustrate the sensitivity of the retrieved density models to assumptions on damping, resulting from the structure of the resolution matrix. However, our particular inversion scheme is non-linear, and therefore involves several iterations, whose results may not be completely represented by the resolution matrix corresponding to the first iteration only. In what follows, we present more complete tests involving the computation of synthetic seismograms and their iterative inversion, more accurately simulating the inversion process corresponding to real spectral data.

Specifically, we are interested in the contaminant signal in density resulting from our iterative inversion scheme. The spatial parameterization and input models of Experiments E and F are revisited in Experiments J and K (radial parameterization $p_{max} = 6$ and $p_{max} = 10$ respectively, Table 1) whereby the estimated models $\mathbf{m}^J_{est}$ and $\mathbf{m}^K_{est}$ are now obtained from inversions of synthetic seismograms computed from input models $\mathbf{m}^J_{true}$=$\mathbf{m}^K_{true}$. $\mathbf{m}^J_{true}$ and $\mathbf{m}^K_{true}$ are composed of models P16B30 for δV_p and SH12WM13 for δV_s, and there are no density perturbations. Aspherical structure up to harmonic degree 12 and radial order 13 are included in the computation of synthetic seismograms. We start the inversions from PREM (*Dziewonski and Anderson, 1981*), and damp the second radial derivative to ensure radial smoothness. η_3 for V_p was required to be twice as strong as for either V_s or ρ to produce a radially smooth model. After 4 iterations, the models $\mathbf{m}^J_{est}$ and $\mathbf{m}^K_{est}$ converge to give 99.6% and 99.5% fits to the synthetic data respectively.

The two models $\mathbf{m}^J_{est}$ and $\mathbf{m}^K_{est}$ are extremely similar and we believe that this is due to the choice of damping to smooth the radial models. At present, the radial damping η_3 applied for V_p is insufficient and stronger damping should be applied. The root-mean-squared profile for $\delta V_{p\,est}$ shows a large bump in the lower mantle which corresponds to a decreased correlation between the input and output V_p models at the same depths (Figs 14a, b, c, and d).

The patterns of $\mathbf{m}^J_{est}$ are shown in Fig. 16 for degrees 1 through 6. The patterns of $\mathbf{m}^K_{est}$ are so similar to $\mathbf{m}^J_{est}$ that we omit their plots. The input model for $\mathbf{m}^J_{true}$=$\mathbf{m}^K_{true}$ is shown in Fig. 15 for comparison. Assessment of our inversion for density with real data, can be made by comparing $\mathbf{m}^J_{est}$ with $\mathbf{m}^J_{true}$. In particular, we can compare the density model obtained from normal mode data (Figs 10c and 11c), with the ghost density patterns in the third column in Fig. 16. Many of the high density features from our density models are also present, both in pattern and amplitude, in the ghost density model. Some of them, of course, could be real, such as high densities beneath the Americas and Asia at most depths in the mantle, where we expect high densities to correlate with high velocities in subduction zones. On the other hand, at the bottom of the mantle, where we cannot rely on our a priori intuitions, the density model inverted from normal modes spectra does not have high density structure in the Pacific and over Africa at 2800 km as do $\delta\rho^J_{est}$ or $\delta\rho^K_{est}$. However, these high density features are present in the density model of SPRD6 (*Ishii and Tromp, 1999*) at this depth.

Discussion and Conclusions

Current methods of retrieving three-dimensional mantle density structure from normal mode spectra (*Kuo and Romanowicz, 1999b*) and normal mode splitting coefficients (*Ishii and Tromp, 1999*) do not appear to yield reliable density models. The mantle density models are affected by the contamination of V_P and V_S structure into the density model space, and depend strongly on the *a priori* starting models in velocity, towards which the inversion is damped, at least for certain choices of depth parameterization.

Resovsky and Ritzwoller, (1999) have documented the instability of ρ models derived from normal mode splitting coefficients when using a sweep of *a priori* constraints. They have shown that it is not possible to determine correlation and/or decorrelation of $\delta\rho$ with seismic velocity as a function of depth. Our work supports their conclusions that current methods and data sets are not sufficient to uniquely determine the density structure of the Earth. We have shown that it is possible to retrieve models of ρ perturbations purely due to contamination from V_S and V_P structure, and that these ghost ρ models are consistent in pattern and amplitude with published ρ models inverted from splitting coefficients (*Ishii and Tromp, 1999*), or with ρ models which we determine from normal mode spectral data, depending on the details of the test performed. We have found that resolution tests involving linear products of resolution matrices with input Earth models devoid of density perturbations ($\mathbf{m}_{true} = [V_p, V_s, 0]$) produce ghost density models which closely resemble the density structure of SPRD6. On the other hand, non-linear inversions of synthetic spectra computed from the same input model $\mathbf{m}_{true} = [V_p, V_s, 0]$ produce a ghost density pattern which resembles density models estimated from normal mode spectral data (*Kuo and Romanowicz, 1999*). It may not be possible to resolve lateral density variations in the mantle independently of those of seismic velocities. However, at least in the upper mantle and down to the mid mantle, reasonable assumptions about positive correlation between densities and seismic velocities can be made on the basis of 1) mineral physics data and 2) geoid fits obtained using seismic velocity models converted into density. Normal mode spectra can therefore be used to constrain the scaling parameter as a function of depth, an issue which we investigate in a forthcoming study.

References

Dziewonski, A.M., X.-F. Liu, and W.-J. Su, in *Earth's Deep Interior: the Doornbos memorial volume*, D. J. Crossley, ed., pp. 11-50, Gordon and Breach Science, Newark, N.J., 1997.

Dziewonski, A.M. and D.L Anderson, Preliminary reference Earth model, *Phys. Earth Planet. Inter.*, **25**, 297-356, 1981.

Giardini, D., X.-D. Li and J.H. Woodhouse, Splitting functions of long-period normal modes of the Earth, *J. Geophys. Res.*, **93**, 13716-42, 1988.

He, X. and J. Tromp, Normal-mode constraints on the structure of the Earth, *J. Geophys. Res.*, **101**, 20053-82, 1996.

Ishii, M. and J. Tromp, Normal-Mode and Free-Air Gravity Constraints on Lateral Variations in Velocity and Density of Earth's Mantle *Science*, **285**, 1231-6, 1999.

Ishii, M. and J. Tromp, Three-dimensional modeling of mantle heterogeneity and their implications for petrology, *Eos Trans. AGU*, **79**, F656, 1998.

Karato, S., Importance of anelasticity in the interpretation of seismic tomography, *Geophys. Research Letters*, **20**, 1623-6, 1993.

Kuo, C., 1999. *Three-dimensional Density Structure of the Earth: Limits fo Astrophsycial and Seismological Approaches*, Ph.D. Thesis, University of California, Berkeley, California.

Kuo, C. and B. Romanowicz, Three-dimensional Density Structure Obtained by Normal Mode Spectral Measurements, *Proceedings, IUGG XXII General Assembly*, A62, 1999a.

Kuo, C. and B. Romanowicz, Density and Seismic Velocity Variations Determined from Normal Mode Spectra, *Eos Trans., AGU*,**80**, S14, 1999b.

Kuo, C., J. Durek and B. Romanowicz, Mantle heterogeneity inferred from normal mode spectra, *Eos, Trans. AGU*, **79**, F627, 1998.

Li, X.-D. and B. Romanowicz, Global mantle shear velocity model developed using nonlinear asymptotic coupling theory. *J. Geophys. Res.*, **101**, 22245-72, 1996.

Li, X.-D., D. Giardini, and J.H. Woodhouse, The relative amplitudes of mantle heterogeneity in P velocity, S velocity and density from free-oscillation data, *Geophys. J. Int.*, **105**, 649-57, 1991.

Masters, G., S. Johnson, G. Laske, and H. Bolton, A shear-velocity model of the mantle. *Philos. Trans. R. Soc. London A*, **354**, 1385-411, 1996.

Panero W. and R. Jeanloz, Mineral phases and density of oceanic crust subducted into the Earth's lower mantle, *in preparation*, 1999.

Resovsky, J.S. and M.H. Ritzwoller, Regularization uncertainty in density models estimated from normal mode data, *Geophys. Res. Lett.*, **26**, 2319-22, 1999.

Resovsky, J.S. and M.H. Ritzwoller, New and refined constraints on three-dimensional Earth structure from normal modes below 3 mHz, *J. Geophys. Res.*, **103**, 783-810, 1998.

Su, W.-J. and A.M. Dziewonski, Simultaneous inversion for 3-D variations in shear and bulk velocity in the mantle, *Phys. Earth Planet. Inter.*, **100**, 135-156, 1997.

Van Der Hilst, R.D., S. Widiyantoro, and E.R. Engdahl, Evidence for deep mantle circulation from global tomography, *Nature*, **386**, 578-84, 1997.

Vasco, D.W. and L.R. Johnson, Whole Earth structure estimated from seismic arrival times, *J. Geophys. Res.*, **103**, 2633-71, 1998.

Table 1. Experiments of input $m_{true} = [\delta V_p, \delta V_s, \delta\rho]$ are tabulated. For all experiments, the same norm damping is used for $\delta V_p, \delta V_s, \delta\rho$ in the determination of m_{est}. The δV_p and δV_s models are from [1]*G. Masters and G. Laske, personal communication*, [2]*Li and Romanowicz, 1996*, [3]*Su and Dziewonski, 1994*.

Experiment	Spatial Parameterization		δV_p^{true} model	δV_s^{true} model		$\delta\rho^{true}$ model		
	$s = 6$ $p = 7$	$s = 6$ $p = 10$	P16B30[1]	SAW12D[2]	SH12-WM13[3]	0	R25	R50
Resolution matrix tests								
A	⋆		⋆	⋆			⋆	
B		⋆	⋆	⋆			⋆	
C	⋆		⋆	⋆		⋆		
D		⋆	⋆	⋆		⋆		
E	⋆		⋆		⋆	⋆		
F		⋆	⋆		⋆	⋆		
H	⋆		⋆	⋆				⋆
I		⋆	⋆	⋆				⋆
Inversions w/ synthetic seismograms								
J	⋆		⋆		⋆	⋆		
K		⋆	⋆		⋆	⋆		

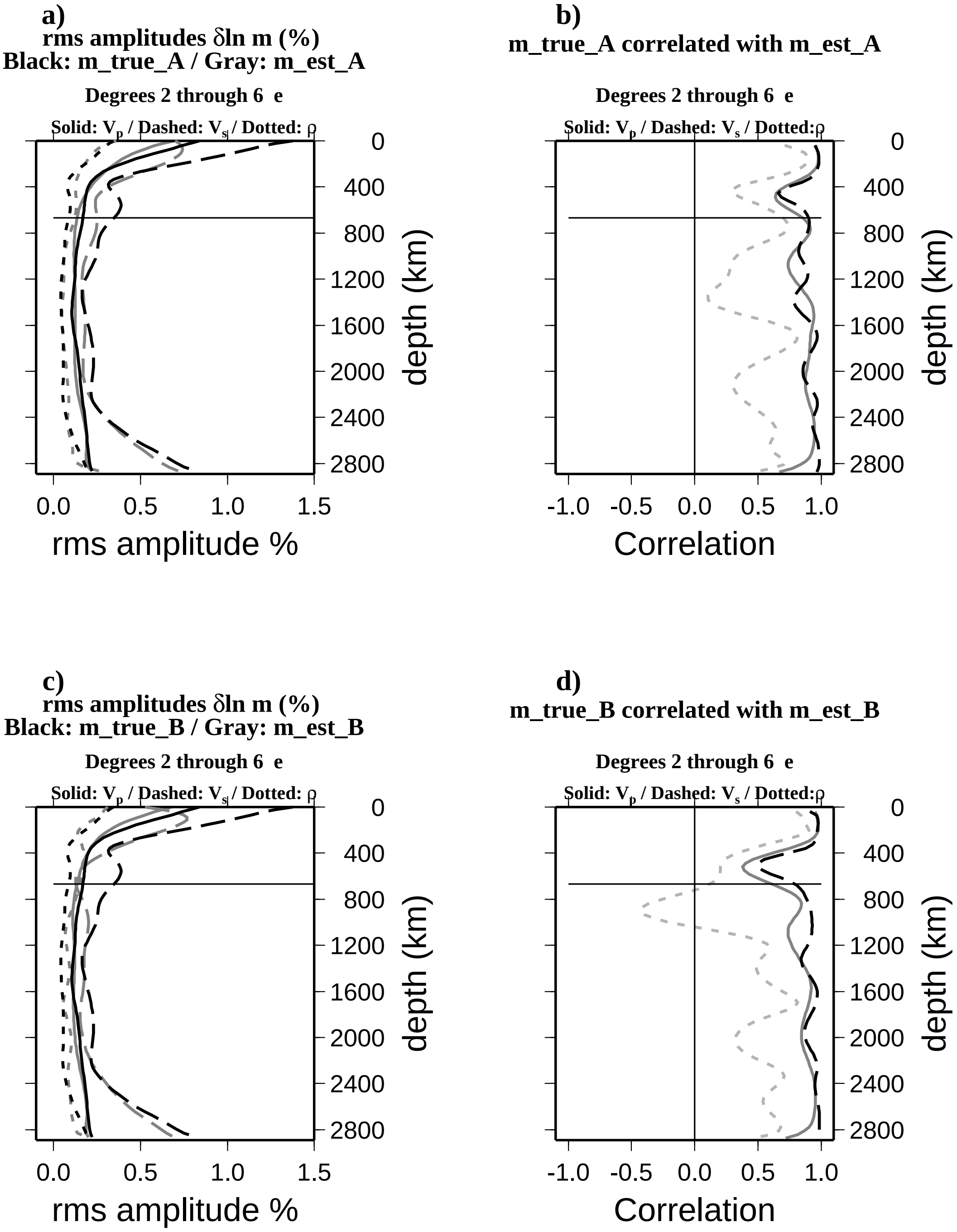

Figure 1. a) For Experiment A, the root mean squared amplitudes of an input model $\mathbf{m}_{true}$ in black lines, and output model $\mathbf{m}_{est}$ from a resolution matrix test, in grey lines. The dashed lines are δV_s, the solid lines are δV_p, and the dotted lines are $\delta\rho$ rms amplitudes. See Table for description of input models. b) The correlation of $\mathbf{m}_{true}$ with $\mathbf{m}_{est}$. The dashed line is the correlation of δV_s between the input and output models, solid line is for δV_p, and the dotted line is for $\delta\rho$. c) & d) same as a) & b), respectively, for Experiment B.

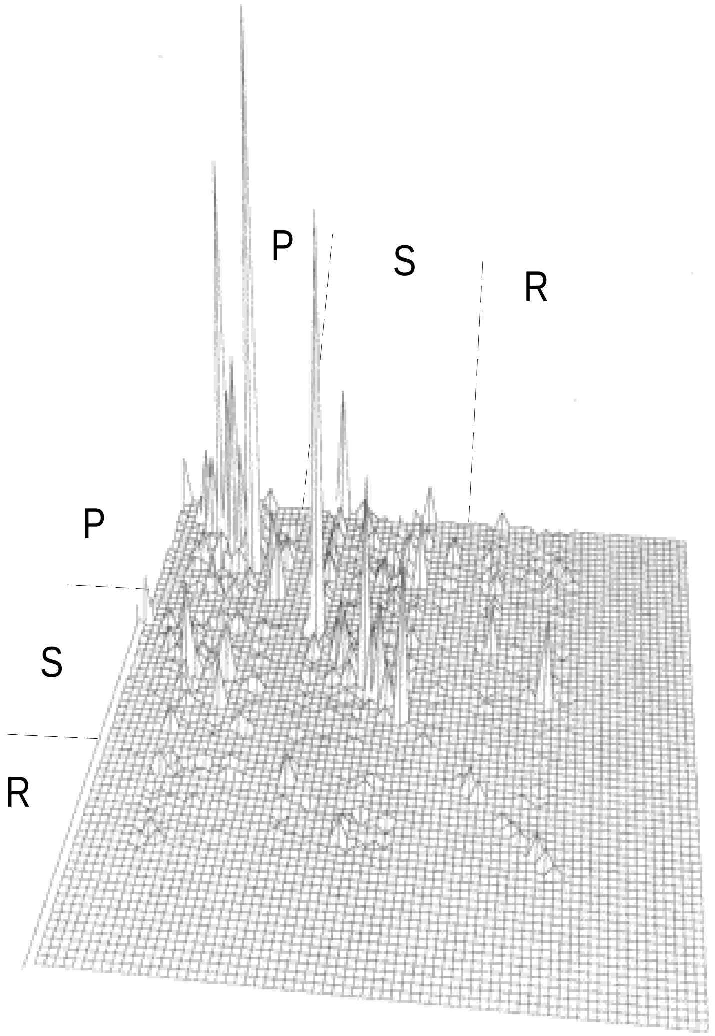

Figure 2. A visualization of a resolution matrix for 44 spheroidal modes used in this study.

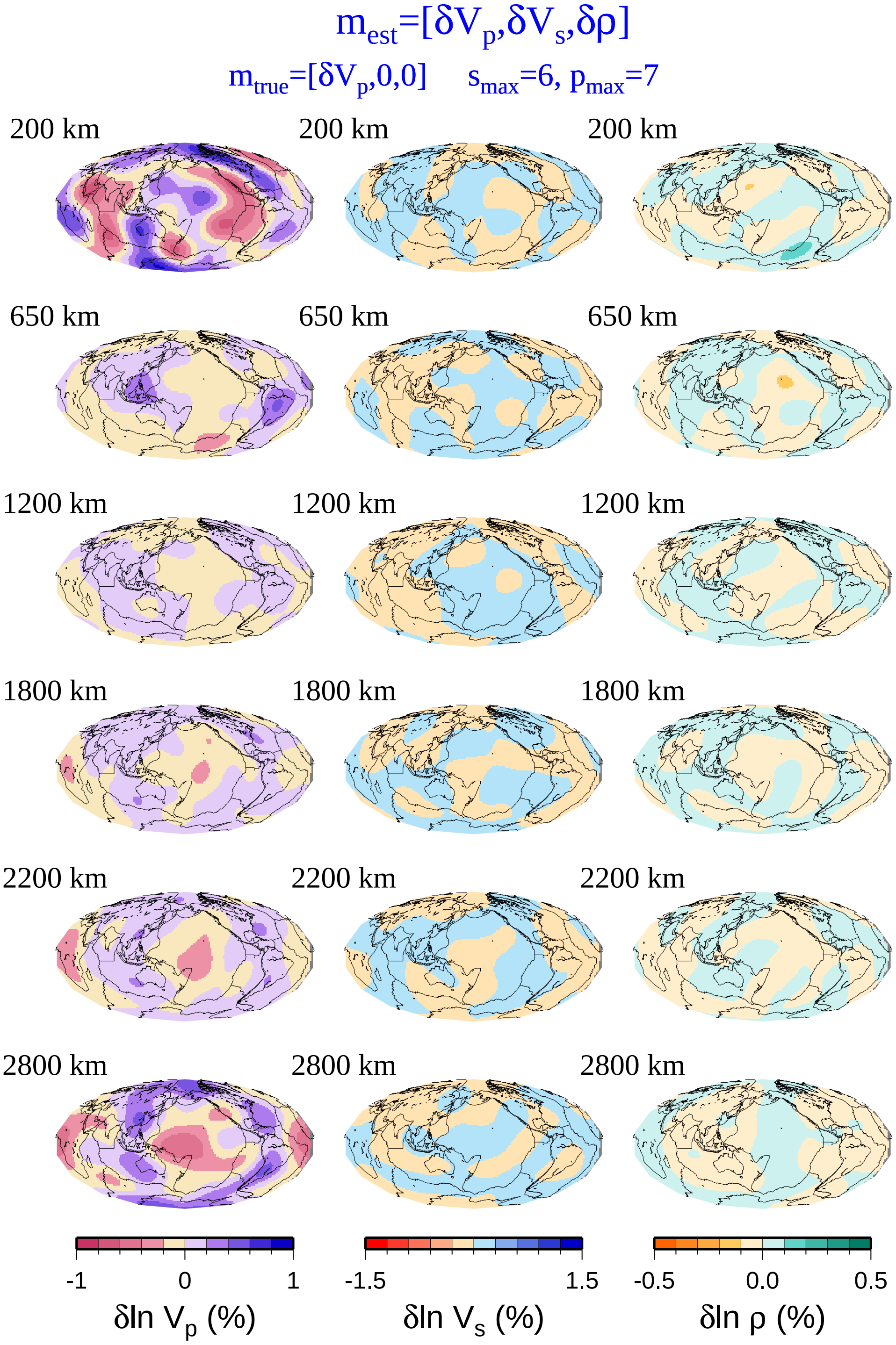

Figure 3. The output model of perturbations in V_p, left column, V_s, middle column, and ρ, right column, for an input model $\mathbf{m}_{true} = [\delta V_p, 0, 0]$, where δV_p is 0.5*SAW12D (*Li and Romanowicz, 1996*). The spatial parameterization for the resolution matrix is $s_{max} = 6, p_{max} = 7$.

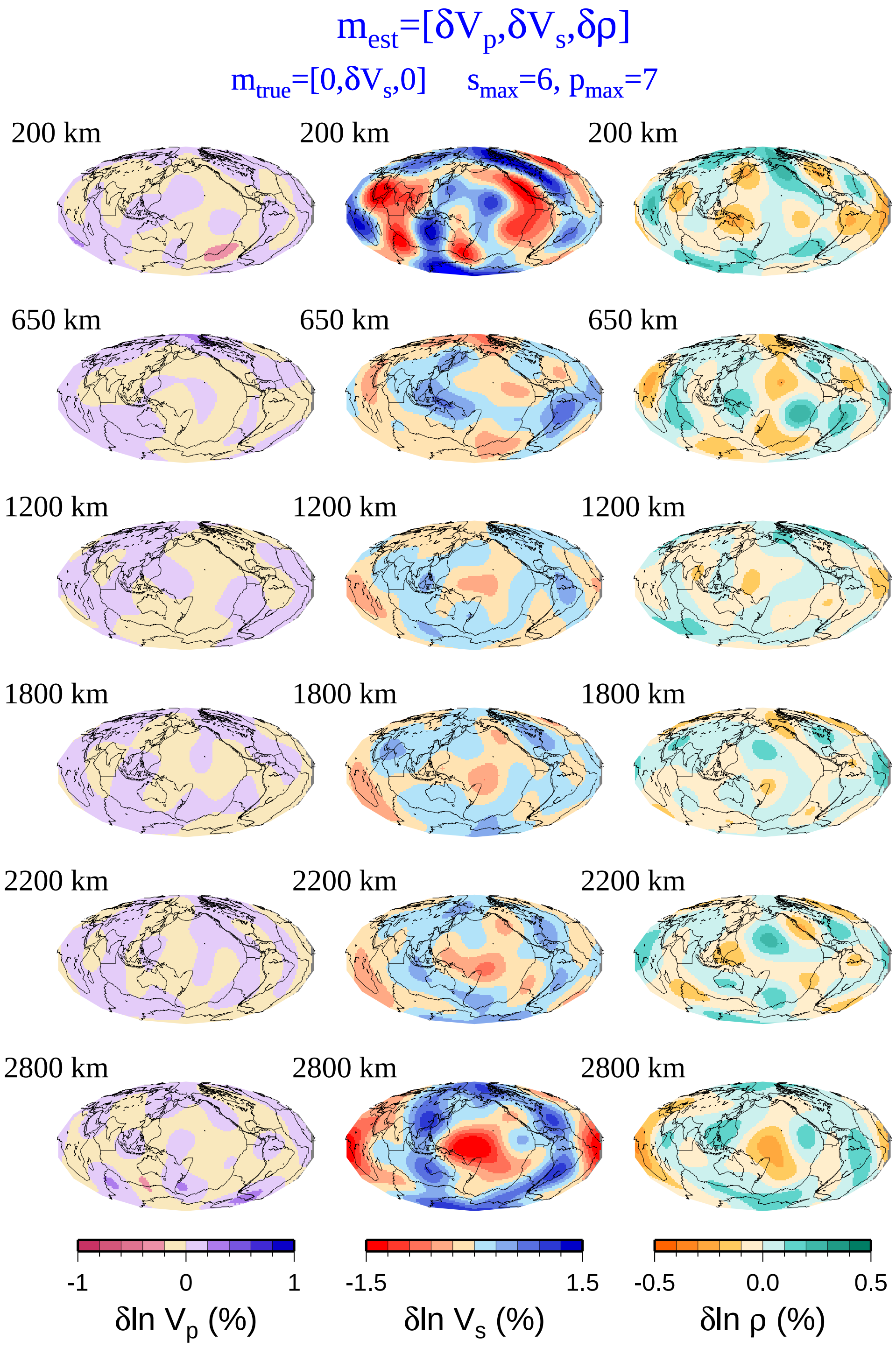

Figure 4. The output model of perturbations in V_p, left column, V_s, middle column, and ρ, right column, for an input model $\mathbf{m}_{true} = [0, \delta V_s, 0]$, where δV_s is SAW12D (*Li and Romanowicz, 1996*). The spatial parameterization for the resolution matrix is $s_{max} = 6, p_{max} = 7$.

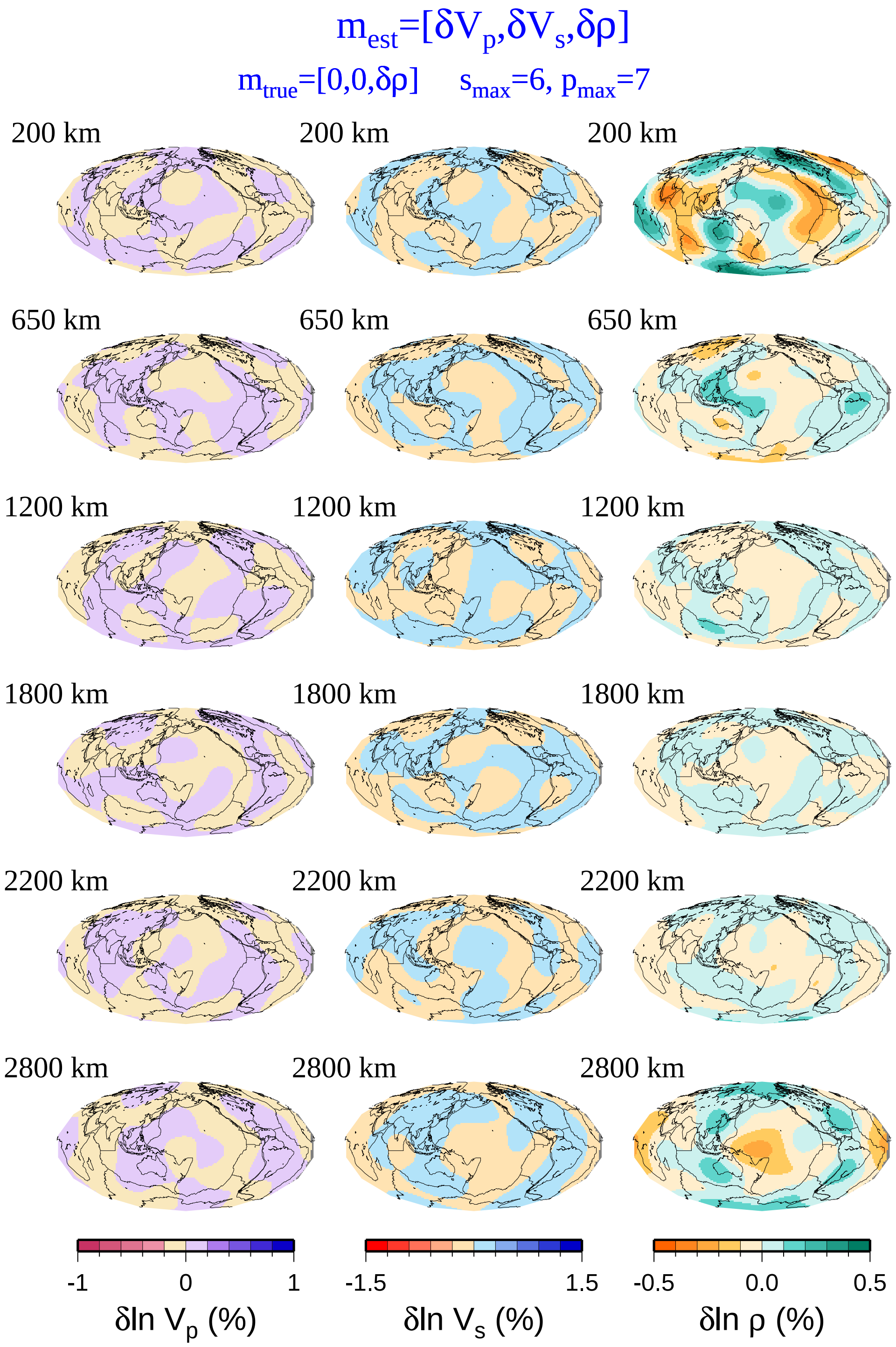

Figure 5. The output model of perturbations in V_p, left column, V_s, middle column, and ρ, right column, for an input model $\mathbf{m}_{true} = [0, 0, \delta\rho]$, where $\delta\rho$ is 0.25*SAW12D (*Li and Romanowicz, 1996*). The spatial parameterization for the resolution matrix is $s_{max} = 6$, and $p_{max} = 7$.

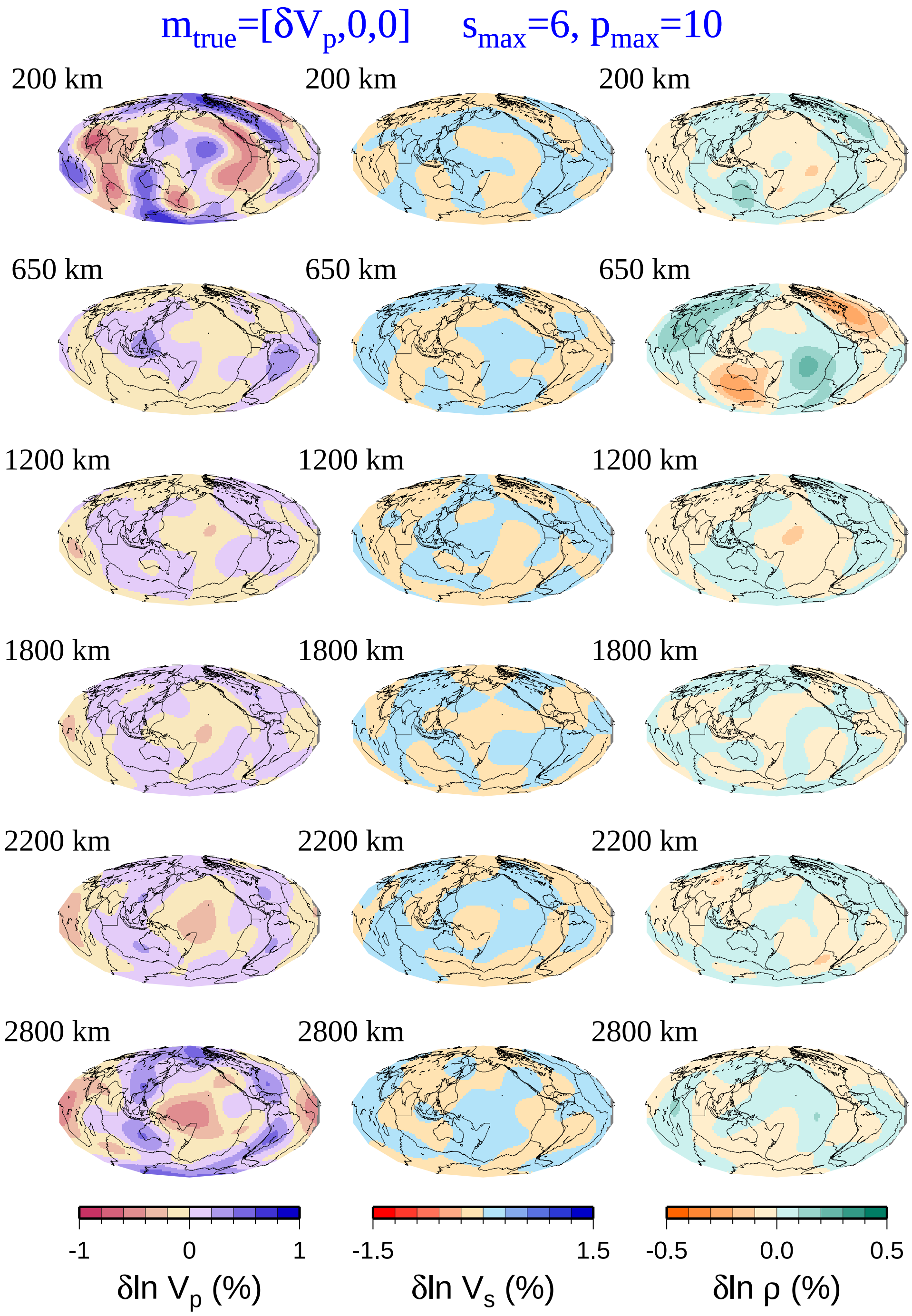

Figure 6. The output model of perturbations in V_p, left column, V_s, middle column, and ρ, right column, for an input model $\mathbf{m}_{true} = [\delta V_p, 0, 0]$, where δV_p is 0.5*SAW12D (*Li and Romanowicz, 1996*). The spatial parameterization for the resolution matrix is $s_{max} = 6, p_{max} = 10$.

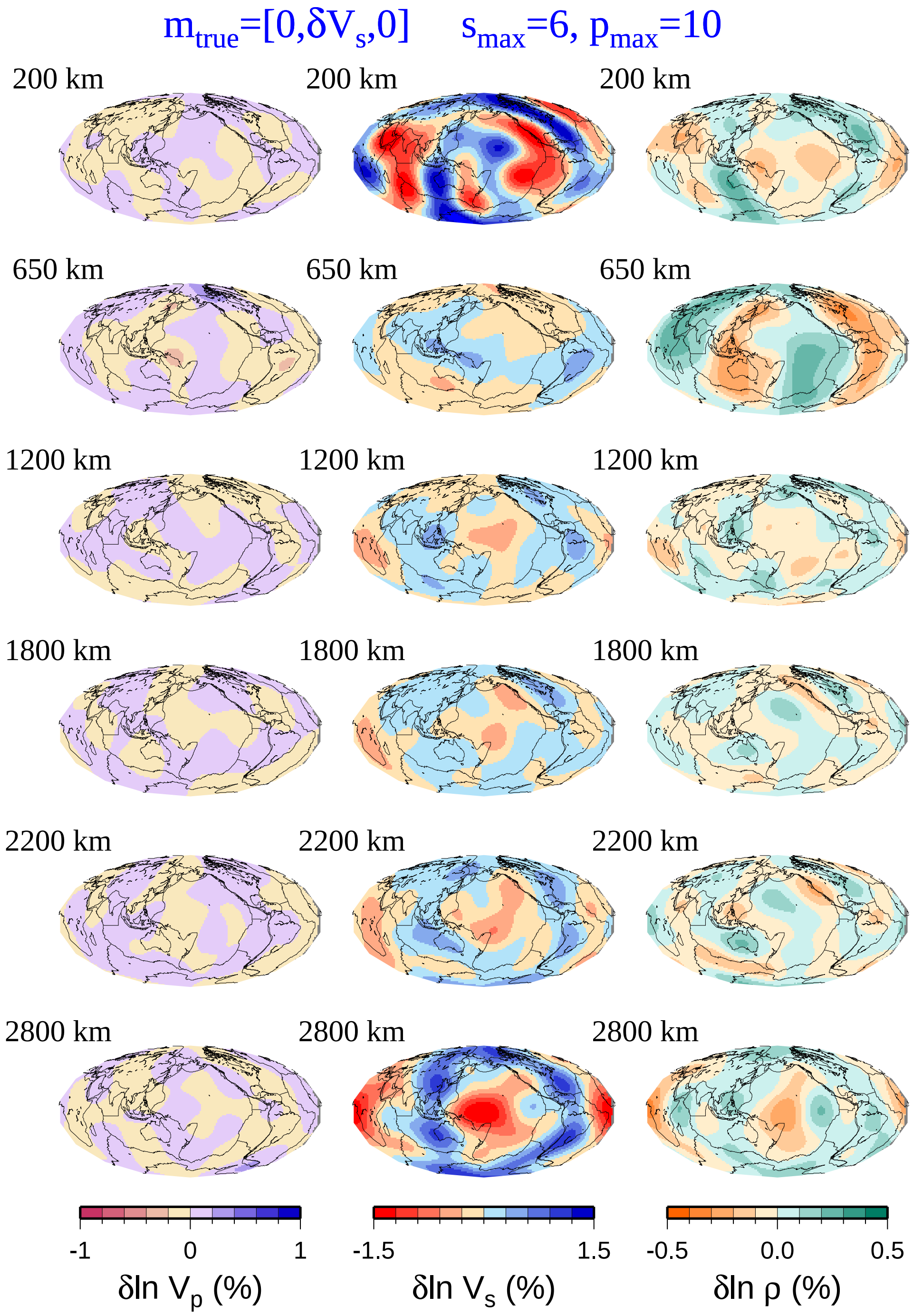

Figure 7. The output model of perturbations in V_p, left column, V_s, middle column, and ρ, right column, for an input model $\mathbf{m}_{true} = [0, \delta V_s, 0]$, where δV_s is SAW12D (*Li and Romanowicz, 1996*). The spatial parameterization for the resolution matrix is $s_{max} = 6, p_{max} = 10$.

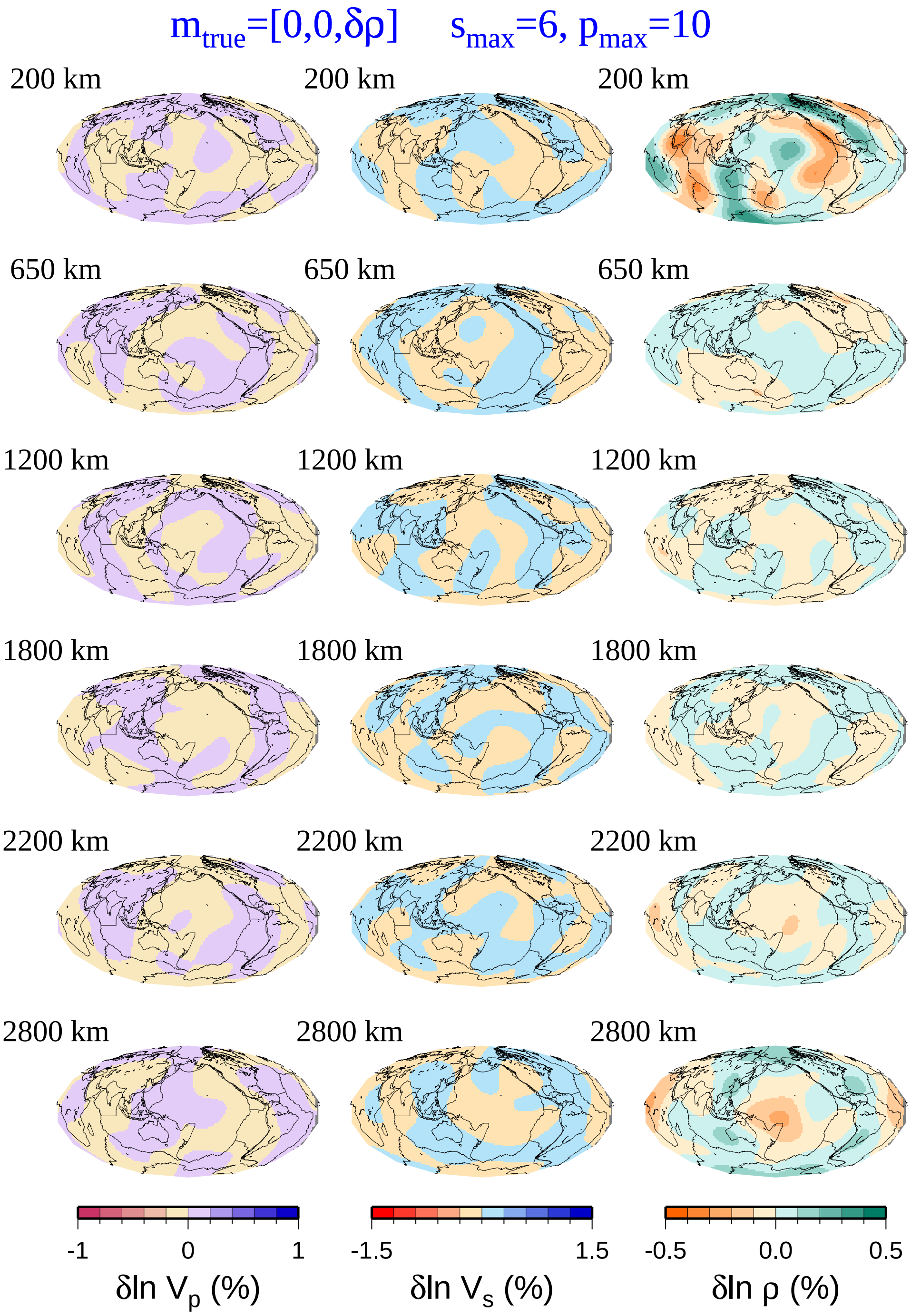

Figure 8. The output model of perturbations in V_p, left column, V_s, middle column, and ρ, right column, for an input model $\mathbf{m}_{true} = [0, 0, \delta\rho]$, where $\delta\rho$ is 0.25*SAW12D (*Li and Romanowicz, 1996*). The spatial parameterization for the resolution matrix is $s_{max} = 6, p_{max} = 10$.

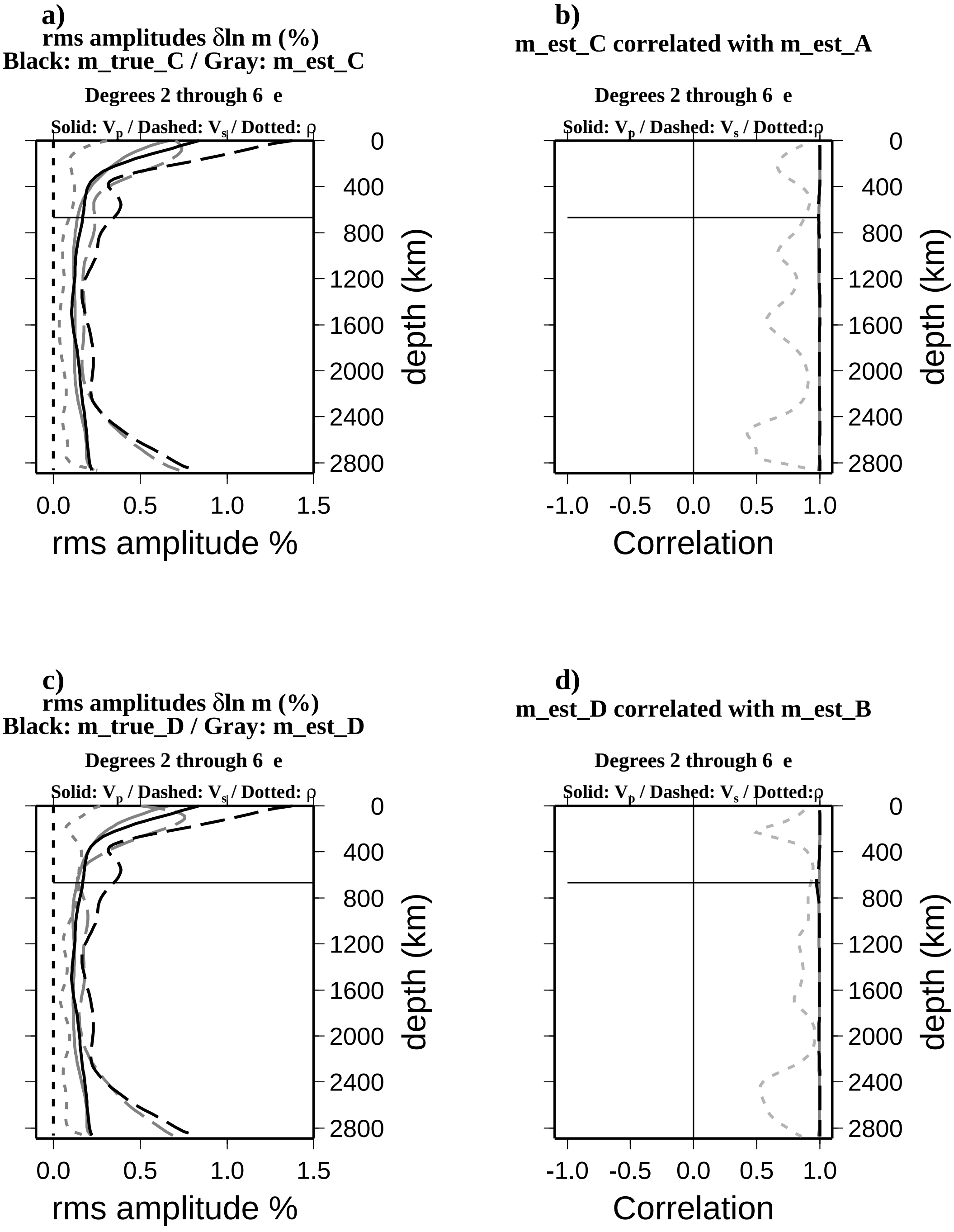

Figure 9. a) For Experiment C, the root mean squared amplitudes of an input model $\mathbf{m}_{true}$ in black lines, and output model $\mathbf{m}_{est}$ from a resolution matrix test, in grey lines. The dashed lines are δV_s, the solid lines are δV_p, and the dotted lines are $\delta\rho$ rms amplitudes. See Table 1 for description of input models. The input $\delta\rho_{true} = 0$ (black dotted line). The retrieved $\delta\rho_{est}$ (grey dotted line) has rms amplitudes > 0. b) The retrieved model $\mathbf{m}^{C}_{est}$ correlated with the retrieved model $\mathbf{m}^{A}_{est}$. c) same as a) for Experiment D. The retrieved $\delta\rho_{est}$ has rms amplitudes > 0. d) The retrieved model $\mathbf{m}^{D}_{est}$ correlated with the retrieved model $\mathbf{m}^{B}_{est}$.

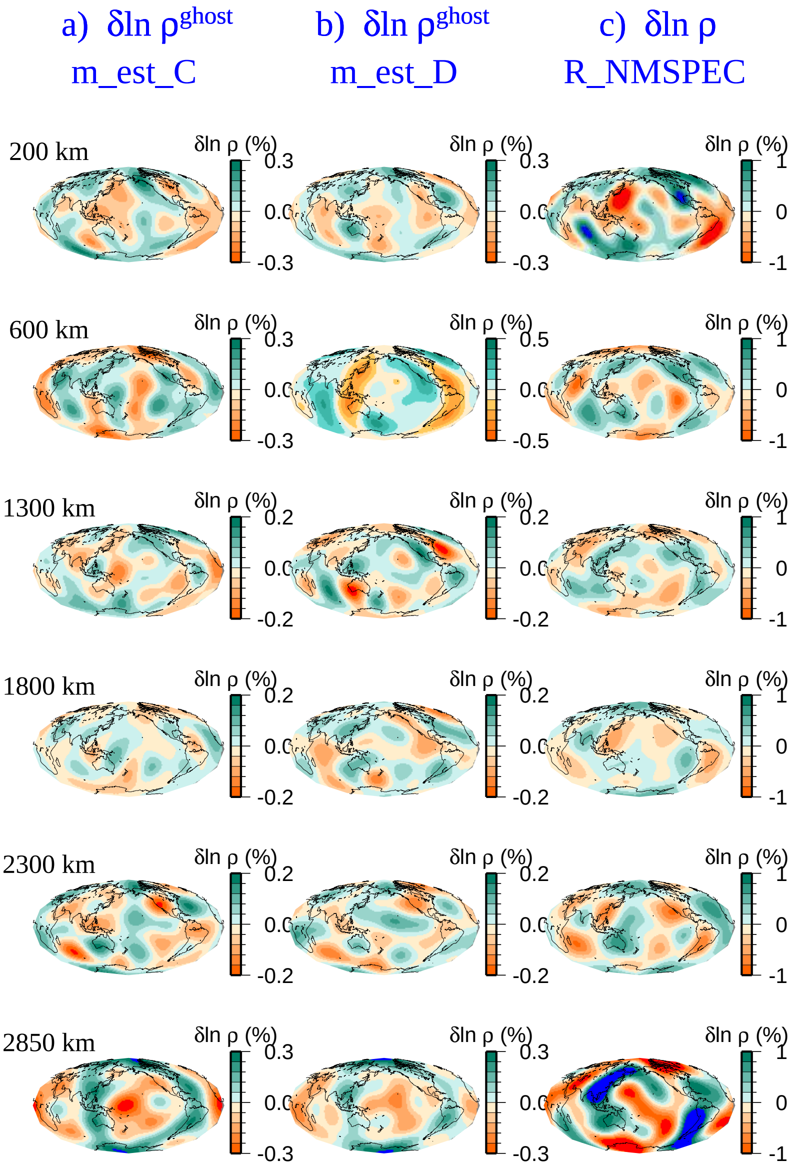

Figure 10. Even degrees 2, 4, and 6 of retrieved model a) $\delta\rho^{C}_{est}$ b) $\delta\rho^{D}_{est}$ are shown for six depths in the mantle. We name $\delta\rho^{C}_{est}$ and $\delta\rho^{D}_{est}$ 'ghost' density models because the input model is $m_{true} = [P16B30, SAW12D, 0]$ for $s_{max} = 6, p_{max} = 7$ and $s_{max} = 6, p_{max} = 10$, respectively. c) The even degrees 2, 4, and 6 of a density model (*Kuo and Romanowicz, 1998, 1999*) retrieved from normal mode spectra is shown for comparison with columns a) and b).

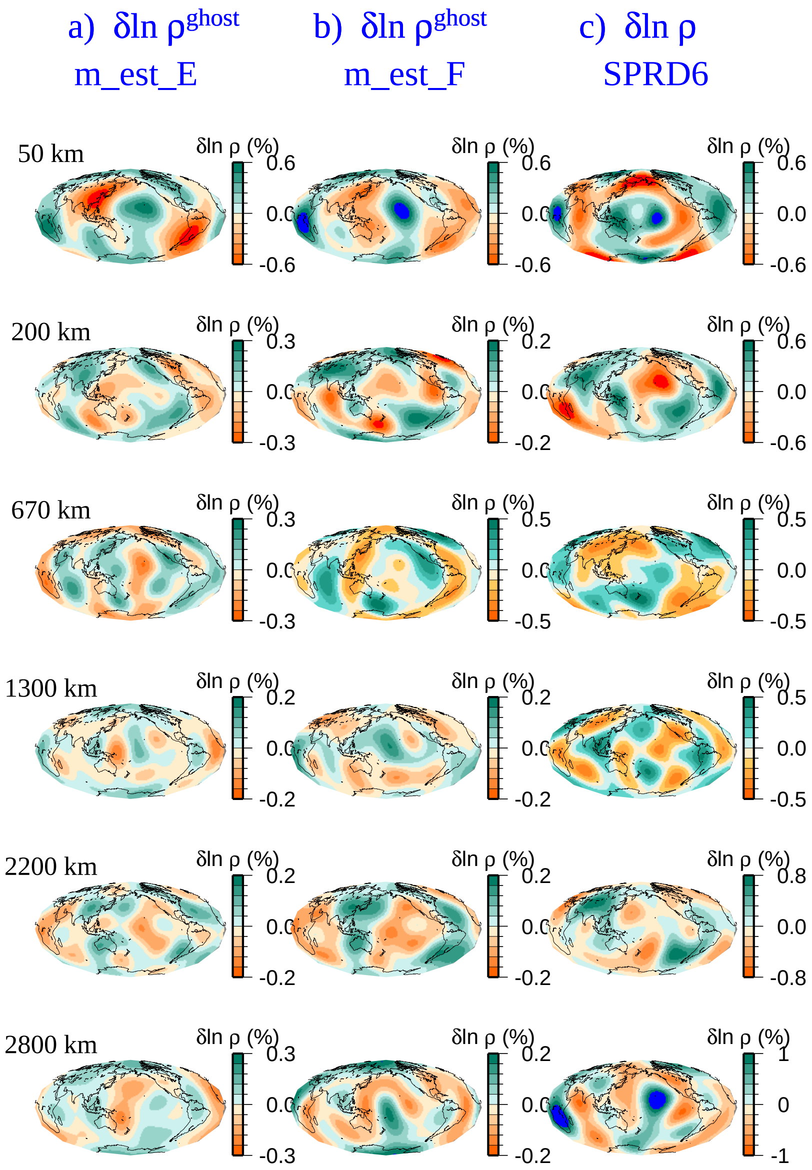

Figure 11. Even degrees 2, 4, and 6 of retrieved model a) $\delta\rho^E_{est}$ b) $\delta\rho^F_{est}$ are shown for six depths in the mantle. We name $\delta\rho^E_{est}$ and $\delta\rho^F_{est}$ 'ghost' density models because the input model is $m_{true} = [P16B30, SH12WM13, 0]$ for $s_{max} = 6, p_{max} = 7$ and $s_{max} = 6, p_{max} = 10$, respectively. c) The even degrees 2, 4, and 6 of the density model of SPRD6 (*Ishii and Tromp, 1999*), at six mantle depths, is shown for comparison with columns a) and b). SPRD6 is inverted from normal mode splitting coefficients.

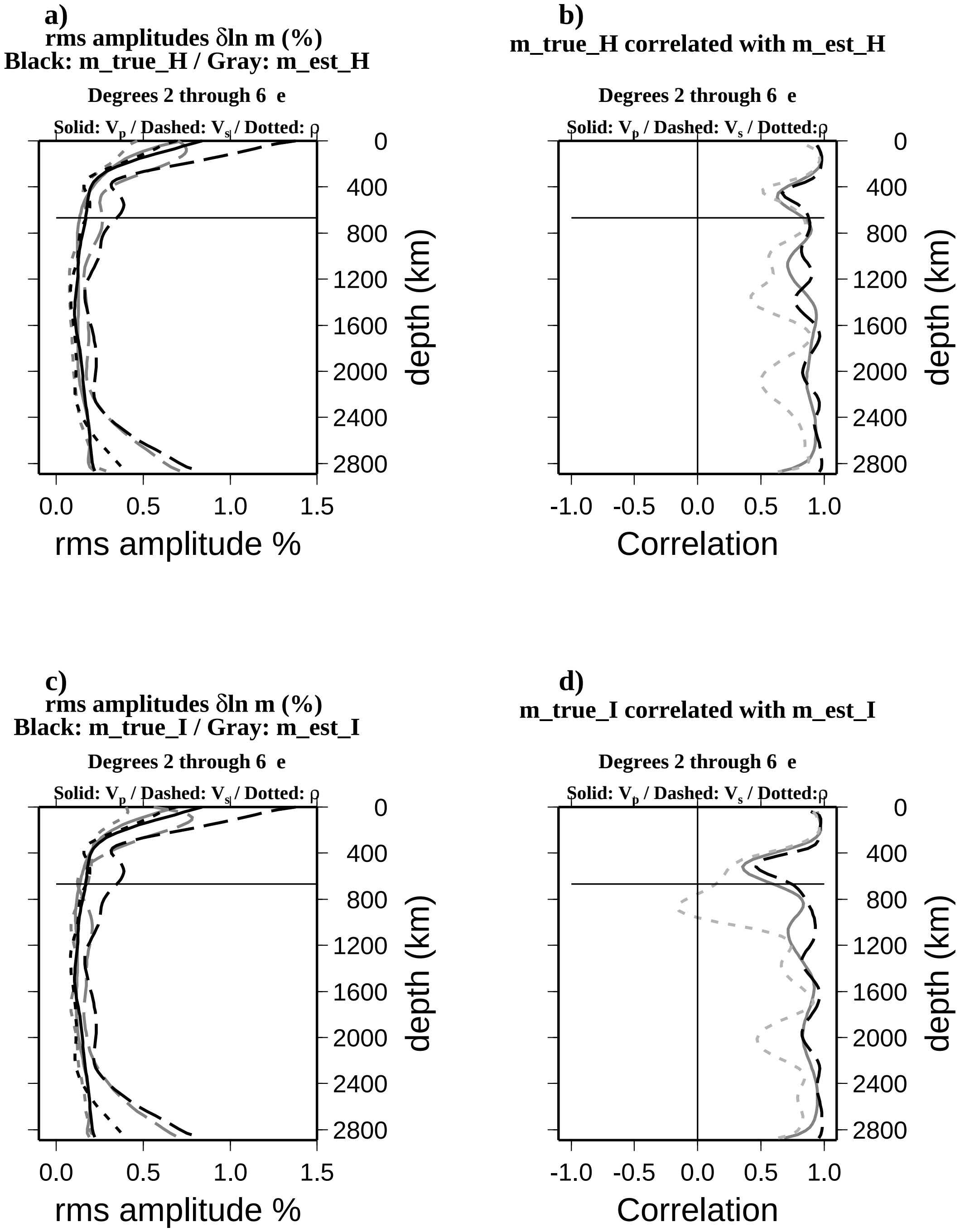

a)
rms amplitudes δln m (%)
Black: m_true_H / Gray: m_est_H

b)
m_true_H correlated with m_est_H

c)
rms amplitudes δln m (%)
Black: m_true_I / Gray: m_est_I

d)
m_true_I correlated with m_est_I

Figure 12. For Experiments H and I, the same as in Fig. 1

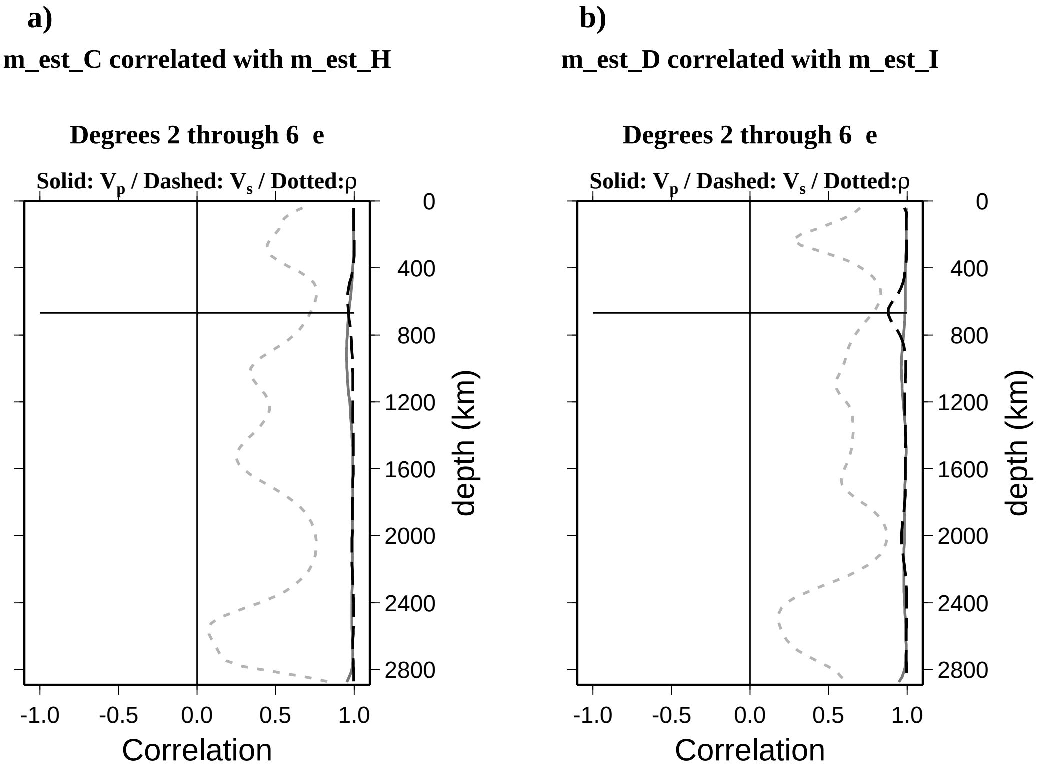

Figure 13. Correlations of estimated models for which input density is zero (Experiments C and D) with estimated models for which input density is a mock model R50 (Experiments H and I). a) Correlation between $\mathbf{m}_{est}^{C}$ and $\mathbf{m}_{est}^{H}$, $s_{max} = 6, p_{max} = 7$, and b) correlation between $\mathbf{m}_{est}^{D}$ and $\mathbf{m}_{est}^{I}$, $s_{max} = 6, p_{max} = 10$.

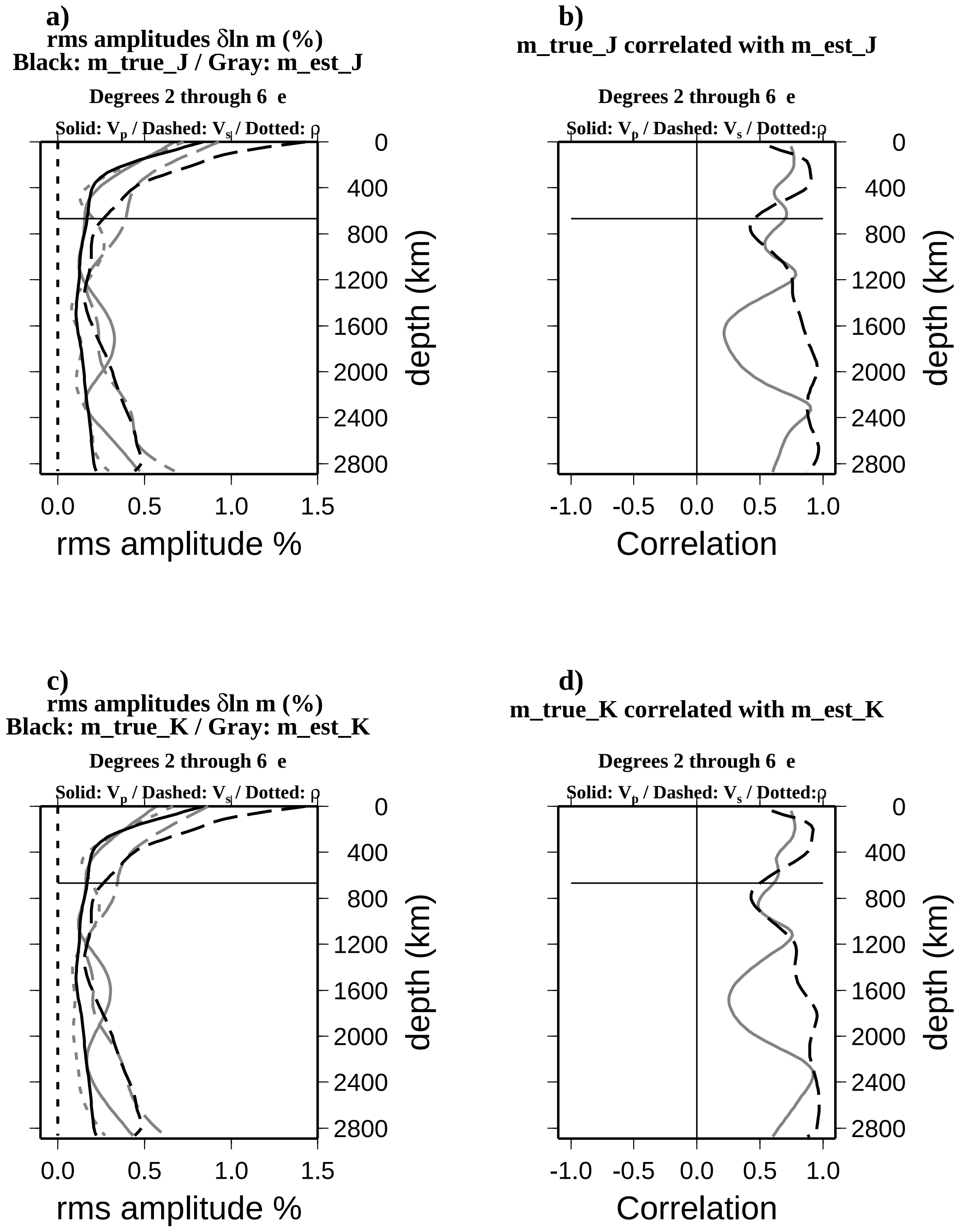

Figure 14. For Experiments J and K, the same as in Fig. 1

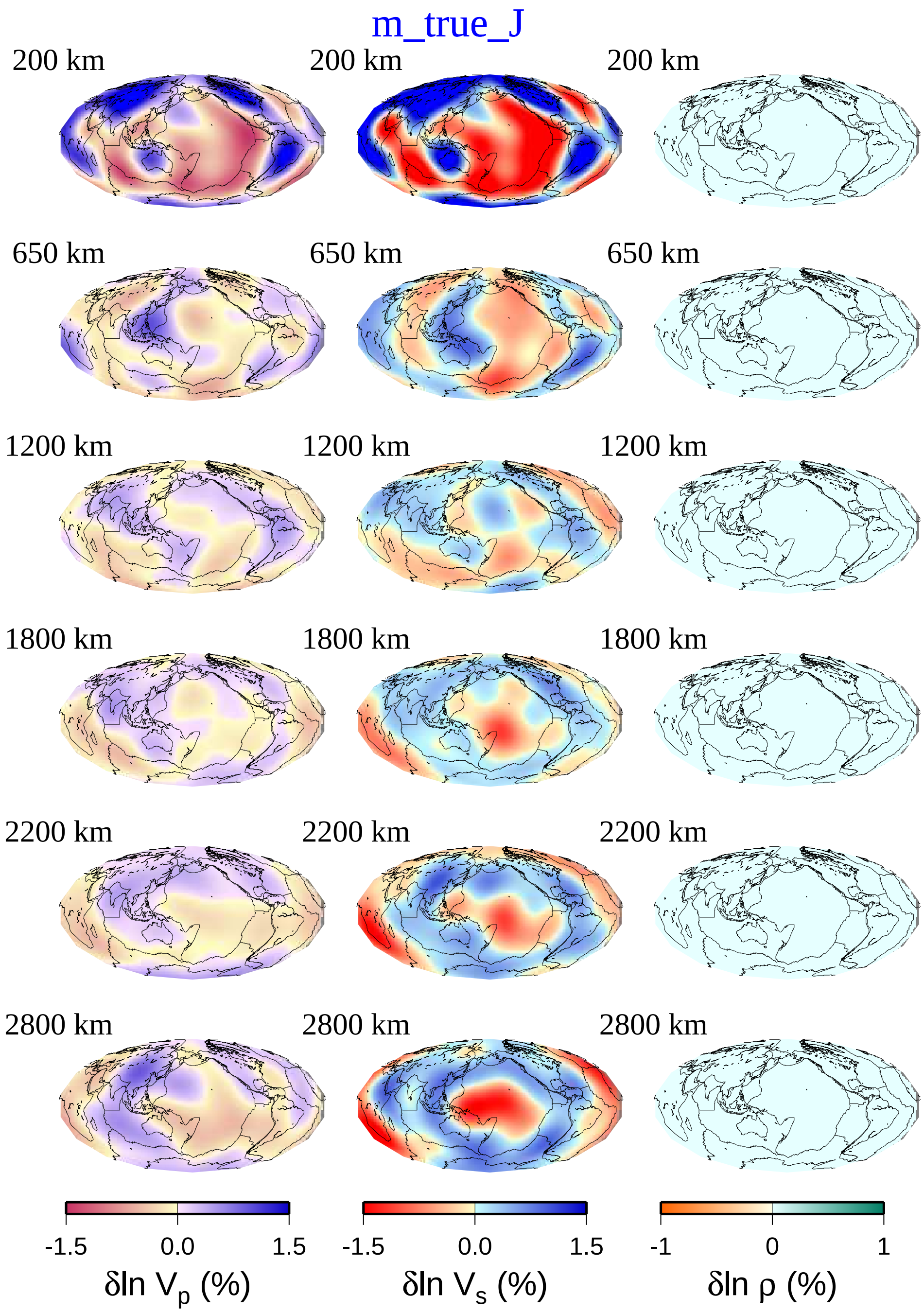

Figure 15. For Experiments J and K (also E and F), the input model $\mathbf{m}_{true} = [\delta V_p, \delta V_s, 0]$ where δV_p=P16B30 (*Masters and Laske, personal communication*), and δV_s=SH12WM13 (*Su and Dziewonski, 1994*). There are no density perturbations in $\mathbf{m}_{true}$.

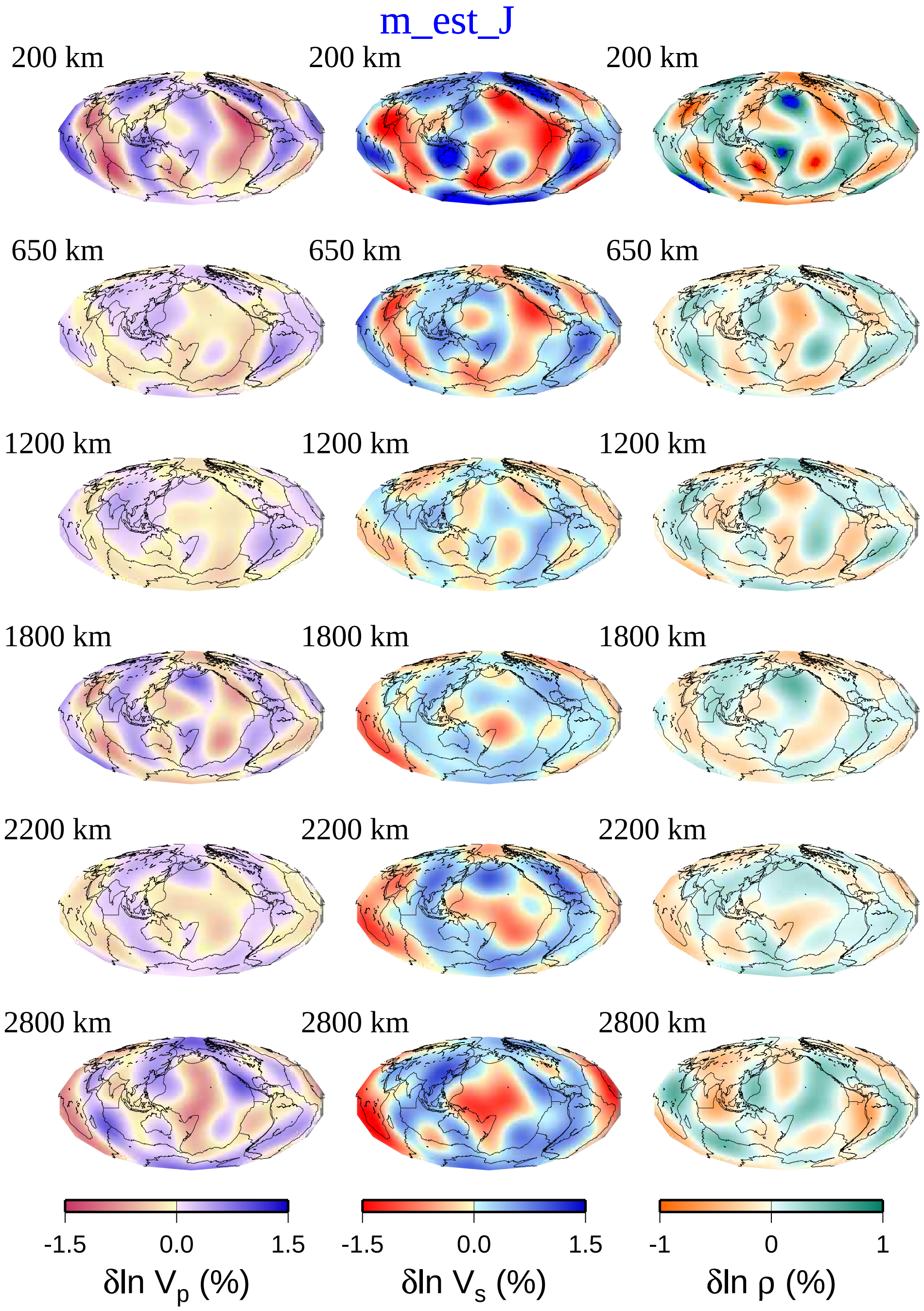

Figure 16. From resolution tests inverting synthetic seismograms, the output model of perturbations in V_p, left column, V_s, middle column, and ρ, right column, for an input model $\mathbf{m}^J_{true}$. The spatial parameterization for this estimated model is $s_{max} = 6, p_{max} = 7$, whereas $s_{max} = 12, p_{max} = 13$ for the input model were used in the synthetic seismogram computations.